Hyperfine Interactions 123/124 (1999) 455–479

Nuclear resonant scattering of synchrotron radiation from thin films

R. Röhlsberger

Fachbereich Physik, Universität Rostock, August-Bebel-Str. 55, D-18055 Rostock, Germany
E-mail: roehle@physik1.uni-rostock.de

The optical properties of thin films containing Mössbauer isotopes undergo dramatic changes in the vicinity of a nuclear resonance. Remarkable phenomena are observed in the energetic and temporal response of X-rays resonantly scattered in grazing incidence geometry. These properties allow an effective discrimination of the resonantly scattered radiation from the nonresonant electronic charge scattering. In contrast to Bragg scattering from single crystals, the reflectivity of film systems can be tailored by their design and the way of preparation. As a result, several optical elements have been developed for ultra-narrow bandpass filtering of synchrotron radiation: Grazing-Incidence Antireflection (GIAR) films, nuclear resonant multilayers and reflection gratings. Moreover, resonant scattering in grazing incidence geometry is a very attractive tool to study properties of thin films themselves. This has led to applications, e.g., in the study of surface magnetism and the determination of vibrational properties of thin films. Such investigations benefit from the outstanding brilliance of third-generation synchrotron radiation sources, extending the sensitivity of the method into the monolayer regime.

1. Introduction

The remarkable properties of nuclear resonant thin film reflection have been realized soon after the discovery of the Mössbauer effect. After a first study of the fundamental aspects [1], a few applications in the study of hyperfine interactions in thin films followed [2–4], taking advantage of the depth sensitivity in grazing incidence geometry. However, due to the low brilliance of radioactive sources, this method did not become very widespread. New momentum to this field was added after the first nuclear resonance excitation with synchrotron radiation [5]. The enormous brilliance of these sources allows one to illuminate surfaces at grazing angles very effectively, opening the possibility to perform surface studies with great sensitivity. Some examples for such studies of thin films via nuclear resonant scattering of synchrotron radiation will be discussed in this contribution.

In the beginning of this rapidly developing field, however, thin films have been applied for novel instrumentation techniques: the use of synchrotron radiation for nuclear resonant scattering experiments is dominated by the problem to reject the huge background of nonresonant electronic charge scattering. After considering electronically forbidden, pure nuclear reflections from perfect single crystals, it was recognized

that also thin films offer a unique way for ultranarrow bandpass filtering [6]. Elaborate thin film designs improve the signal-to-noise ratio by orders of magnitude and particularly allow tailoring the reflectivity according to the experimental needs.

Three types of grazing incidence optical elements have been developed so far for nuclear resonant filtering of synchrotron radiation: grazing incidence antireflection (GIAR) films, nuclear resonant multilayers and nuclear reflection gratings. In each case the layer system contains a Mössbauer isotope whose structure function is different from that of the whole layer system. The overall structure is designed for suppression of the nonresonant reflectivity while maintaining a high reflectivity over a large bandwidth around the nuclear resonance. Indeed, these elements have been shown to provide a reduction of the nonresonant reflectivity of up to three orders of magnitude and transmit an energy bandwidth in the μeV range with peak reflectivities close to unity.

This paper is organized as follows: in section 2, some fundamental properties of grazing incidence reflection with special emphasis on nuclear resonant scattering are reviewed. Section 3 introduces several types of grazing incidence optical elements that have been mentioned above. Besides general design considerations, experiments are described in which the performance of these elements is demonstrated. The last section deals with selected applications in which thin films themselves are characterized by elastic and inelastic nuclear resonant scattering.

2. Characteristics of grazing-incidence resonant scattering

The striking effects of nuclear resonant scattering from thin films are discussed here in terms of an optical model where the index of refraction of the material is considered. This allows one to explain the broadening of the energy response in grazing incidence geometry that leads to a strong speedup of the decay of the collectively excited nuclear state. The interference between electronic and nuclear scattering leads to an interesting angular dependence of the delayed resonant reflectivity.

2.1. Index of refraction

For X-rays the complex refractive index of any material can be written as $n = 1 - \delta - \mathrm{i}\gamma$, where $\delta \approx 10^{-5}$–10^{-6} and $\gamma \approx 10^{-6}$–10^{-10} for X-rays in the 10 keV range. Since the X-ray index of refraction for every material is below unity, matter is optically thinner than vacuum and total reflection occurs for X-rays incident below the critical angle $\varphi_c \approx \sqrt{2\delta}$.

Significant changes are introduced when the X-ray energy approaches the vicinity of a nuclear resonance. For a general account of the theory of resonant grazing incidence reflection, see, e.g., [7]. In order to discuss the typical effects in the most simple way, we assume the case of unsplit nuclear levels, where the nuclei in the films

act as single line scatterers[1] with a resonant energy E_0. This is the case to a good approximation in nonmagnetic alloys like stainless steel, which will be taken here as an example, referred to as Fe_2Cr_2Ni. The index of refraction for this material, as it is derived from the forward scattering amplitude, is given by

$$n = 1 + \frac{2\pi}{k_0^2} \sum_u \rho_u \left[-Zr_0 + \mathrm{i}\frac{k_0}{4\pi}\sigma_\mathrm{t} + \frac{f_0}{x - \mathrm{i}} \right]_u =: 1 - (\delta_\mathrm{e} + \delta_\mathrm{n}) - \mathrm{i}(\gamma_\mathrm{e} + \gamma_\mathrm{n}), \quad (2.1)$$

where $x = -2(E - E_0)/\Gamma_0$ and the sum runs over all constituents of the alloy, denoted by the subscript u. ρ_u is the atomic number density, Z the atomic number, r_0 the classical electron radius, σ_t the total absorption cross-section and f_0 the nuclear scattering length. The term $f_0/(x - \mathrm{i})$ is the complex Lorentzian frequency distribution of a single nuclear resonance. The subscripts e and n denote the contributions from electronic and nuclear resonant scattering, respectively. Considering only the real part of the refractive index, the critical angle for a single-component material reads

$$\varphi_\mathrm{c} = \sqrt{2(\delta_\mathrm{e} + \delta_\mathrm{n})} = \sqrt{\frac{Zr_0\rho\lambda^2}{\pi} - \frac{f_0\rho\lambda^2}{\pi}\frac{x}{x^2 + 1}}\,. \quad (2.2)$$

(We have neglected here the contribution due to inner-shell resonant scattering that becomes appreciable in the vicinity of absorption edges.) Exactly at resonance the critical angle is not well defined due to the large imaginary contribution to the scattering amplitude. The energy dependence of the nuclear contributions δ_n and γ_n for $^{57}Fe_2Cr_2Ni$ is shown in figure 1(a). The electronic contributions δ_e and γ_e are drawn as dotted lines. In addition, the energy dependence of the phase of the reflection coefficient of $^{57}Fe_2Cr_2Ni$ at the critical angle is shown in figure 1(b). This will play an important role in the description of nuclear resonant scattering from reflection gratings, see section 3.3.

Due to the large nuclear contribution to the refractive index, the critical angle for total reflection around the resonance is much larger than far off the resonance. This is illustrated in figure 1(c), where the reflectivity is displayed in the (φ, E)-plane and the regions are shaded where the reflectivity exceeds the value 0.5. The contour of this region can be considered as a plot of the critical angle vs. energy around the resonance. This already allows one to discriminate the nuclear scattered radiation from the nonresonant electronic charge scattering: there is a region of angles of incidence at which the nonresonant radiation deeply penetrates into the medium while the resonant radiation is nearly totally reflected. A further increase in suppression can be gained with a layer system especially designed for destructive interference of the nonresonant radiation, in which at least one layer contains resonant nuclei. This will be discussed in section 3.1.

[1] In the presence of a magnetic hyperfine interaction, strong polarization mixing effects are introduced. The corresponding 2×2 matrix that represents the scattering amplitude in this case is described in [7].

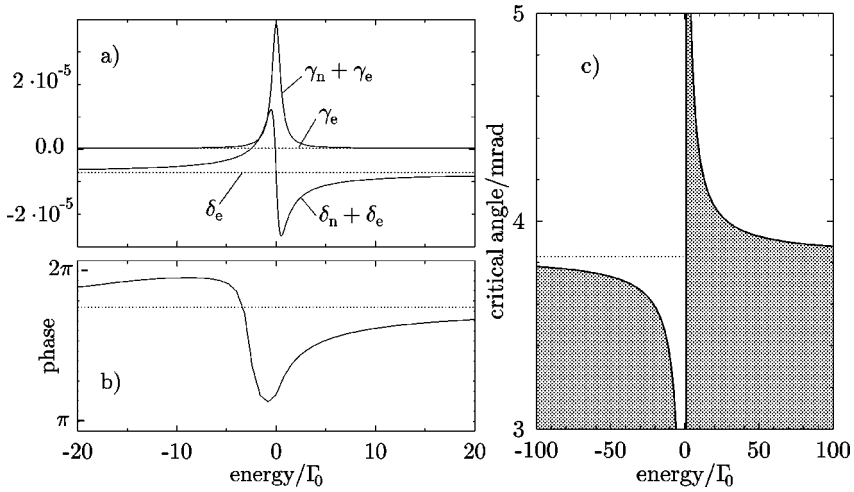

Figure 1. (a) Index of refraction (real and imaginary part) of $^{57}Fe_2Cr_2Ni$ in the vicinity of the nuclear resonance. (b) The phase of the Fresnel reflection coefficient. (c) Reflectivity plotted in the (φ, E)-plane. The regions where $|R_{01}(\varphi, E)|^2 > 0.5$ are shaded. The dotted line marks the nonresonant value of φ_c.

2.2. Angular dependence of delayed resonant scattering

Total reflection in grazing incidence geometry is a true two-beam case of dynamical diffraction that is essentially the (0 0 0) Bragg reflection, where the critical angle can be taken as the Darwin width of the Bragg peak. This kind of Bragg reflection is allowed for any material, regardless of its structure, since it falls within the limit of forward scattering. Due to the presence of strong charge scattering, pronounced interference effects with the nuclear scattering are encountered. This interference leads to a peculiar angular dependence of the delayed resonant scattering that will be investigated here.

Usually, the reflectivity of a layer system is evaluated as a function of energy around the nuclear resonance. The time response is then obtained via Fourier transform. The reflection coefficient of a single layer (1) of thickness d_1 on a semi-infinite substrate (2) is given by [7,8]

$$r(\varphi, E) = \frac{r_{01} + r_{12}\mathrm{e}^{2\mathrm{i}k_{1,z}d_1}}{1 + r_{01}r_{12}\mathrm{e}^{2\mathrm{i}k_{1,z}d_1}}, \tag{2.3}$$

where r_{01} and r_{12} are the Fresnel reflection coefficients of the boundaries, which are given by

$$r_{ij} = \frac{\beta_i - \beta_j}{\beta_i + \beta_j} \quad \text{with} \quad \beta = \sqrt{1 + \frac{2(\delta + \mathrm{i}\gamma)}{\varphi^2}}, \tag{2.4}$$

where the energy dependence is contained in δ and γ according to eq. (2.1). $k_{i,z} = \beta_i k_{0,z}$ is the z-component of the wavevector in layer i, as expressed by the z-component $k_{0,z}$ of the incident wavevector.

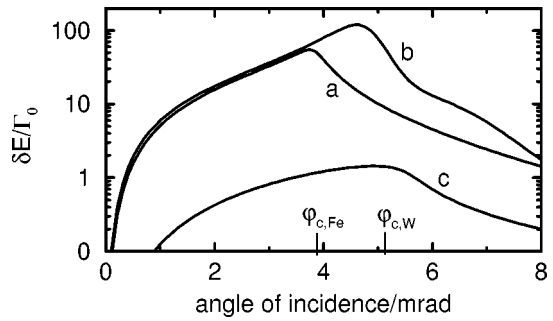

Figure 2. Intensity of nuclear resonant scattering from stratified media according to eq. (2.5): (a) the surface of semi-infinite ^{57}Fe, (b) a 10 nm thick layer of ^{57}Fe on W, and (c) an ultrathin layer of 0.3 nm ^{57}Fe on W. The ^{57}Fe was assumed to be polycrystalline. The intensity peaks at angles between the electronic critical angles of Fe and the substrate material W.

According to Parseval's theorem, the total time-integrated delayed intensity can be expressed by an integration over the energy response:

$$\delta E(\varphi) = \int_{-\infty}^{\infty} \left| r(\varphi, E) - r_{\mathrm{e}}(\varphi) \right|^2 \mathrm{d}E, \tag{2.5}$$

where $r_{\mathrm{e}}(\varphi)$ denotes the reflectivity of the layer system far off the nuclear resonance. For a discussion of the angular dependence, eq. (2.5) has been evaluated for the following cases:

(a) the surface of semi-infinite ^{57}Fe,

(b) a 20 nm thick layer of ^{57}Fe on W, and

(c) an ultrathin layer of 0.3 nm ^{57}Fe on W.

The results are displayed in figure 2. With increasing thickness of ^{57}Fe, the delayed reflectivity peaks at angles that are shifting from the critical angle of W, $\varphi_{\mathrm{c,W}}$, to the critical angle of Fe, $\varphi_{\mathrm{c,Fe}}$. This can be qualitatively understood in terms of standing waves that form above total reflecting surfaces due to the interference of incident and reflected waves. At the critical angle an antinode of the standing wave coincides with the reflecting surface, leading to an enhanced signal from resonantly scattering adsorbates and ultrathin films. Standing waves also form within thin films on total reflecting substrates if the angle of incidence is located between both critical angles of the film and the substrate.

These theoretical considerations have been confirmed in an experiment involving a layer of 20 nm ^{57}Fe deposited on a glass substrate [9], which corresponds to case (a) discussed here.

The angular dependence of the delayed response is an important property to be observed in thin film and surface studies via nuclear resonant scattering. The proper choice of the incident angle allows one to obtain maximum intensity in a scattering experiment. This will be demonstrated in experiments that are discussed in section 4.

3. Grazing incidence optics for nuclear resonant filtering

As already mentioned, grazing incidence reflection can be treated as the Bragg (0 0 0) reflection that is an allowed reflection independent of the structure of the material. However, with a proper choice of a layered system and incidence angle, the structure factor of the electronic reflection can be made zero. This is a brief description of an antireflection coating that allows one to create pure nuclear reflections in grazing incidence geometry. This section describes various ways how the electronic structure factor of thin-film systems can be significantly reduced and how strong reflectivity around the nuclear resonance can be achieved. In contrast to pure nuclear Bragg reflections, where the properties are determined by the diffracting crystals and cannot be changed, nuclear resonant scattering from thin films can be tailored to the experimental needs by preparing the films accordingly. Several techniques are available today that allow deposition of thin films in almost any desired composition and structure.

3.1. GIAR-films

A significant suppression of the nonresonant electronic charge scattering can be achieved by a grazing-incidence antireflection (GIAR)-film, i.e., a coating layer on the surface designed for destructive interference of the nonresonant radiation. In the most simple case a GIAR-film consists of a single coating on a semi-infinite substrate. The basic idea of GIAR-films was already brought up before the first nuclear scattering experiment with synchrotron radiation was carried out [6]. The theory of GIAR-films has been developed in a series of papers [10,11], the main results of which will be summarized in this section.

The main goals of the GIAR-film design are a strong suppression of the nonresonant scattering and a broad energy response around the nuclear resonance. For use in a subsequent nuclear scattering experiment, the GIAR-film should preserve the properties of synchrotron radiation as much as possible. The good collimation is maintained by using substrates that are extremely smooth on all length scales. These are commercially available in very good quality and many different sizes. Particular attention has to be paid to preserve the time structure. Since the monochromatization proceeds via nuclear resonant scattering with a finite lifetime, this property can only be preserved approximately. The best approximation would be a scattering process with an energy width ΔE corresponding to a lifetime $\Delta t = \hbar/\Delta E$ that is below the time resolution of the detector. If we assume a typical time resolution of 1 ns for fast X-ray detector systems [12,13], this leads to an energy width of $\approx 140\Gamma_0$ ($= 0.65$ μeV) in case of the 14.4 keV resonance of ^{57}Fe. We will see in the following sections that the energy response of GIAR-films can be broadenend to such values. Coincidentally, this fulfills another important requirement, namely, for a bandwidth that allows to excite all (hyperfine-split) resonances in a given material simultaneously.[2] These conditions can

[2] The known hyperfine interactions at the ^{57}Fe nucleus cover approximately this range.

only be fulfilled if the nuclei in the GIAR-film do not exhibit hyperfine interactions, so that the scattering strength is concentrated in one single resonance line.

3.1.1. Electronic suppression

The layer thickness and the angle at which destructive interference occurs is derived from the condition

$$r_{01} + r_{12} e^{2ik_{1,z}d_1} = 0. \tag{3.1}$$

This relation basically represents two equations, one for equal amplitudes of the outgoing waves and one for these waves to be in antiphase, i.e., the phase shift to be an odd multiple of π. In a simple picture of two waves emerging from the layer system, this situation is displayed in figure 3(a). The amplitude condition can only be fulfilled if $|r_{12}| > |r_{01}|$. This means that the reflectivity from the inner boundary must be higher than the reflectivity from the surface boundary to compensate for the absorption of the beam going through the coating. This can only be achieved if the substrate consists of the material with the higher electron density ρ_e. The resonant nuclei can be either in the substrate or in the coating. However, to minimize absorption losses, the reso-

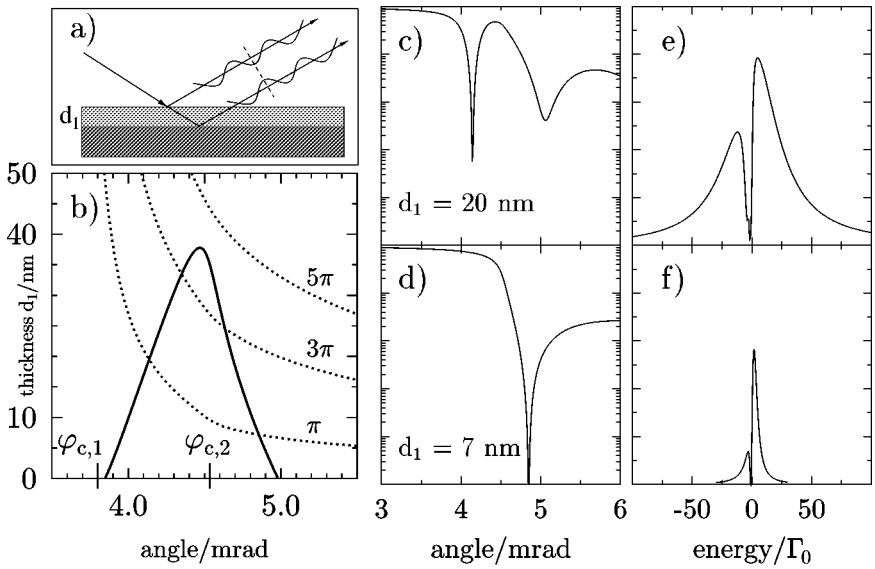

Figure 3. (a) Two-beam interference at an antireflection coating. (b) Graphical solution for the film thickness and the angle of incidence required for an antireflection coating at 14.4 keV (Fe_2Cr_2Ni on Pd). The bell-shaped curve represents the condition for equal amplitudes, the hyperbola-shaped curves the condition for the relative phase to be an odd multiple of π. Intersection points mark the simultaneous fulfillment of both conditions. The critical angles for Fe_2Cr_2Ni ($\varphi_{c,1}$) and Pd ($\varphi_{c,2}$) are marked on the abscissa. (c) and (d) Rocking curves of the reflectivity for the films belonging to the intersection points of lowest order with $d_1 = 20$ nm (damping-stabilized film) and $d_1 = 7$ nm (impedance-matched film). (e) and (f) Energy spectra of the reflectivity of both films at the minimum of the electronic reflectivity. The vertical scale ranges from 0 to 1.

nant nuclei should be in the coating. The following considerations apply only to this case.

Values for the proper layer thickness yielding destructive interference can be found graphically by plotting the conditions resulting from eq. (3.1). This is shown in figure 3(b) for the system Fe_2Cr_2Ni on Pd. The intersection points indicate the simultaneous solution of both equations by one pair of values (d_1, φ). The critical angles of total reflection for Fe_2Cr_2Ni and Pd are marked on the abscissa. One class of solutions lies between both critical angles. According to the nomenclature of Hannon et al. [10] these are called the "damping-stabilized" solutions, since they would not be present in the case of zero absorption in the coating. The absorption is necessary to damp the strong reflectivity of the substrate in order to get equal amplitudes of the outgoing waves, as sketched in figure 3(a). The solutions which lie beyond both critical angles are called the "impedance-matched" solutions. While damping-stabilized solutions exist for every absorbing coating material with an electron density $\rho_{\text{e,coating}} < \rho_{\text{e,substrate}}$, the existence of impedance-matched solutions is restricted to $\rho_{\text{e,substrate}}/2 < \rho_{\text{e,coating}} < \rho_{\text{e,substrate}}$ [10].

In general, the angular width of damping-stabilized minima is smaller than that of impedance-matched minima. This is due to different layer thicknesses in both cases: The geometrical phase difference between the beams reflected from the two boundaries of the coating changes by an amount of $4\pi(d_1/\lambda)\Delta\varphi$ when the angle of incidence is changed by $\Delta\varphi$. Therefore the condition of destructive interference is violated more rapidly for thicker coatings when the angle of incidence is varied.

3.1.2. Nuclear bandwidth

Another important property of GIAR-films is the width of the energy response at the minimum of the electronic reflectivity. For a given coating/substrate configuration there is a significant difference between damping-stabilized and impedance-matched GIAR-films. This is illustrated in figures 3(e) and (f), where the energy spectra of the Fe_2Cr_2Ni/Pd based damping-stabilized and impedance-matched GIAR-film belonging to the lowest-order intersection points in figure 3(b) are shown. The bandwidth δE according to eq. (2.5) of the damping-stabilized GIAR-film is about 10 times larger than that of the impedance-matched GIAR-film. In general, the reflective bandwidth of a nuclear resonant layer system increases with decreasing angle of incidence. To illustrate this property, the contour line for $|R|^2 = 0.5$ of semi-infinite $^{57}Fe_2Cr_2Ni$ has been plotted in the (φ, E)-plane, see figure 1(c). In this graph the regions are shaded in which the reflectivity exceeds the value of 0.5. The energetic range within which the reflectivity of $^{57}Fe_2Cr_2Ni$ exceeds this value increases if the angle of incidence approaches the critical angle φ_c (dotted line). The GIAR-films with φ_{min} closest to φ_c are the damping-stabilized films. Therefore, these films are the recommended devices for nuclear broadband filtering.

A remarkable feature is the gap in the reflectivity energy spectra of GIAR-films, i.e., a region of low reflectivity a few natural linewidths below the exact resonance

energy. This is explained by two facts: first, in this region the sum $\delta_e + \delta_n$ goes through 0, see figure 1(a). This means an enhanced transparency, and without absorption the material would be completely transparent. At $E - E_0 = 0$, $\delta_e + \delta_n$ goes through 0 as well, but due to the strong nuclear absorption no minimum is observed there. Second, at energies slightly below the resonance the index of refraction takes a value suitable for destructive interference of the radiation, which again results in a minimum in the energy spectrum. Both effects are responsible for the appearance of the gap in the energy spectrum of the reflectivity.

In general, the angular width $\delta\varphi$ of the minimum and the energy bandwidth δE are related reciprocally. This means that an increase in energy bandwidth is only gained via a decrease in the angular width. A quantitative formulation of this relation has been derived in [14]:

$$\delta\varphi\delta E = \frac{\lambda^2 \rho f_0}{2\varphi_{\min}} \sqrt{q}\,\Gamma_0, \tag{3.2}$$

where ρ is the density of the coating, $\varphi_{\min}$ is the angular location of the minimum and q is the requested level of electronic suppression. Since $\varphi_{\min}$ appears in the relation, this relation is not independent of the layer materials chosen. It is of course valid also for all other Mössbauer isotopes. An overview over possible broadband (damping-stabilized) GIAR-films for other low-energy nuclear resonances is given in table 1 with calculated values for the angular width $\delta\varphi$ of suppression and the width δE of the energy response. With impedance-matched GIAR-films it is in general not possible to excite all lines of a magnetically split hyperfine spectrum simultaneously. However, bandwidths of a few Γ_0 needed for selective excitation of single lines or quadrupole doublets can be obtained together with a strong reduction of the nonresonant reflectivity.

The $^{57}Fe_2Cr_2Ni$-based GIAR-films that have been used as a tutorial example in this paper have been prepared and used in experiments. They were characterized by Mössbauer reflectometry with a conventional source as well as with synchrotron

Table 1
Broadband GIAR-films (1st order damping-stabilized solution) for some Mössbauer isotopes. These films are close to the optimum that is possible for the particular isotope. In each case the f_{ML} is a typical value that is observed at room temperature. The enrichment was assumed to be 100%. $\delta\varphi$ is the angular range along which $|R_{012}|^2 < 0.001$. δE is the integrated nuclear reflectivity according to eq. (2.5).

Isotope	E_0 (keV)	Γ_0 (neV)	f_0 (10^{-12})	f_{ML}	Coating	d_1 (nm)	Sub-strate	$\varphi_{\min}$ (mrad)	$\delta\varphi$ (μrad)	δE (Γ_0)
^{57}Fe	14.4	4.7	1.49	0.75	Fe_5B_4C	31.7	Ta	3.31	8.00	135
^{119}Sn	23.9	25.7	1.35	0.4	SnO_2	42.2	Pd	2.06	1.67	127
^{161}Dy	26.7	16.2	0.95	0.4	Dy_2O_3	29.2	Ta	2.06	3.67	63
^{149}Sm	22.5	64.1	0.55	0.4	Sm_2O_3	25.0	Pd	2.55	4.71	4.4
^{181}Ta	6.23	0.07	0.42	1.0	Ta_2O_5	16.5	Ta	9.68	60.0	9.9
^{151}Eu	21.5	47.0	0.21	0.4	EuO	26.8	Ta	2.53	6.00	6.4
^{169}Tm	8.41	114	0.09	1.0	TmAl	27.5	Ta	5.92	16.7	1.9

radiation [16,17]. With respect to broadband filtering, the optimum matrix material for damping-stabilized GIAR-films is the material with the lowest Z reasonably available, which would be Be. For the design of a ^{57}Fe based broadband GIAR-film, however, B_4C has been chosen, which is not very far from that optimum. This material is known to yield very smooth layers, and therefore it is widely used in sputtering applications, especially for the production of X-ray multilayer monochromators.

3.1.3. Broadband filtering of synchrotron radiation

Based on Fe_5B_4C, the first-order damping-stabilized GIAR-film has been prepared that is a promising candidate for nuclear broadband filtering. After deposition of a Ta substrate layer on a superpolished glass-ceramics (ZERODUR), Fe_5B_4C layers enriched to 95% in ^{57}Fe were produced by rf-sputtering. Conversion electron Mössbauer measurements revealed the Fe_5B_4C to be nonmagnetic. Residual hyperfine interactions, however, are responsible for a quadrupole splitting and broadening of the resonance line [14]. The density of sputtered Fe_5B_4C layers, as determined from the critical angle of total reflection, was found to be 5.2 g/cm^3. With this value the coating thickness of the first-order damping-stabilized solution for Fe_5B_4C/Ta-based GIAR-films is 32.0 nm. A minimum in the electronic reflectivity of $|R|^2 = 0.03$ was found at $\varphi_{\min} = 3.11$ mrad, measured with an angular divergence of the incident radiation of 20 μrad. With an angular divergence of 5 μrad, a value of $|R|^2 = 0.005$ can be expected. In order to analyze the energy spectrum of the reflectivity of the Fe_5B_4C/Ta damping-stabilized GIAR-film, the $^{57}FeBO_3$(3 3 3) pure nuclear reflection [18] has been employed [19]. An external field of about 0.1 T was applied perpendicular to the scattering plane so that the fields of the two antiferromagnetically coupled sublattices were oriented in the scattering plane parallel to the projection of $\vec{k}_0$ on the crystal surface. The quantum beat spectrum and the energy spectrum of the $^{57}FeBO_3$(3 3 3) reflection are shown in figures 4(a) and (c). The dominating quantum beat period, $T_B = 8.8$ ns, is caused by the interference of the outer lines in the spectrum at $\pm 50\Gamma_0$. Due to the orientation of the magnetic fields at the nuclei, the $M = 0$ transitions at $\pm 30\Gamma_0$ are not excited but become apparent by absorption. The expected energy spectrum of the GIAR-film reflectivity is shown in figure 4(c) as a dashed curve. It was calculated assuming a Lamb–Mössbauer factor of 0.75. Due to the gap in the spectrum of the GIAR-film, one line of the $^{57}FeBO_3$ spectrum is only weakly excited. The measured quantum beat spectrum of the combined setup (GIAR-film + $^{57}FeBO_3$ reflection) is shown in figure 4(b). Clearly the high frequency quantum beats of figure 4(a) are also present in figure 4(b), indicating the coherent broadband excitation of the $^{57}FeBO_3$(3 3 3) reflection. Obviously, there is a significant difference to the expected spectrum (dashed line). The energy bandwidth is $\delta E = 110\Gamma_0$ instead of $135\Gamma_0$. This can only be explained by a recoilfree fraction $f_{ML} = 0.5$ in $^{57}Fe_5B_4C$.

Broadband GIAR-films have found a number of applications so far. With the above GIAR-film, nuclear resonant forward scattering from a polycrystalline Fe foil could be observed [19]. Moreover, the electronic suppression provided by a GIAR-

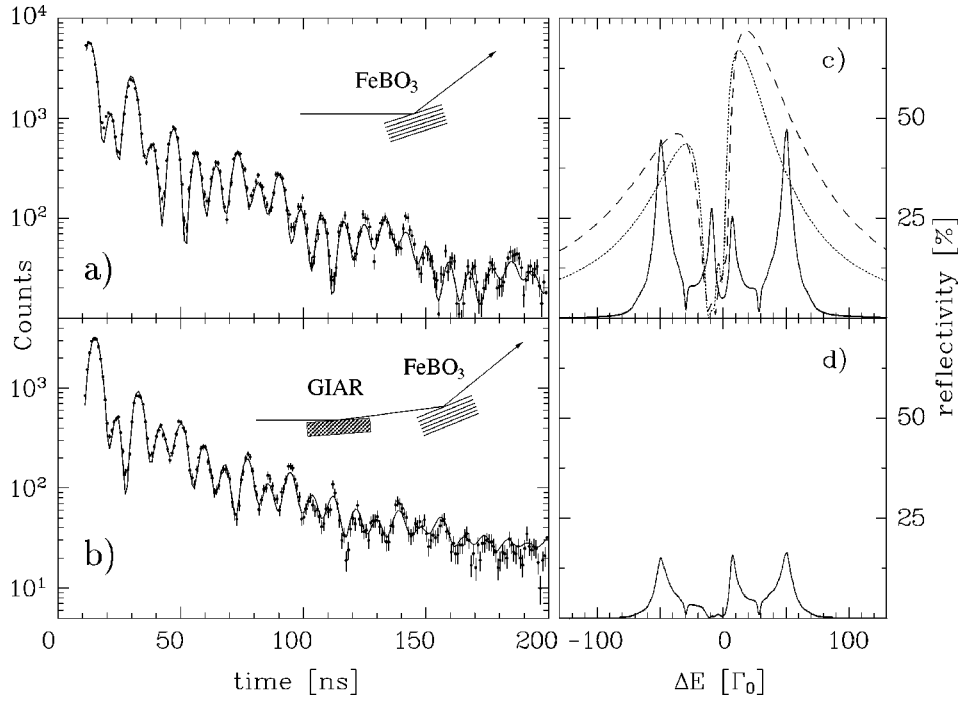

Figure 4. Time and energy spectra of the $^{57}FeBO_3$(3 3 3) reflection excited via an Fe_5B_4C/Ta-based damping-stabilized GIAR-film. (a) Measured time spectrum of the $^{57}FeBO_3$(3 3 3) reflection excited by SR of uniform intensity. (b) Measured time spectrum of the $^{57}FeBO_3$(3 3 3) reflection excited after preceding diffraction of SR at the GIAR-film. (c) Energy spectrum of the $^{57}FeBO_3$(3 3 3) reflection (solid line) as derived from the evaluation of the time spectrum in (a). The dashed and dotted lines are the energy spectra of the GIAR-film reflectivity, for $f_{ML} = 0.75$ and for $f_{ML} = 0.50$, respectively. (d) Energy spectrum of the combined $^{57}FeBO_3$(3 3 3) and GIAR-film reflection, as derived from the evaluation of the time spectrum in (b). The solid lines in (a) and (b) are fits according to the dynamical theory as implemented in the program package CONUSS[3] [21].

film played an essential role in the first observation of the 23.8 keV resonance of ^{119}Sn [20].

3.1.4. Measurement of the reflection phase

As has already been shown in section 2.1, the phase of the reflected radiation varies rapidly in the vicinity of a nuclear resonance. In this section it will be demonstrated how relative phases in the energy response of a resonant scattering process can be measured. The method relies on the detection of the temporal shift of a quantum beat pattern that is due to the change of the relative phase between energetically separated resonances.

[3] A program has been developed for calculation of nuclear resonant scattering from thin films and multilayers that builds on the program package CONUSS [21]. It is available free of charge from the author.

A careful look at the quantum beat pattern in figure 4(b) reveals a shift relative to the pattern in figure 4(a) by ∼2 ns. This is caused by relative phase changes introduced by the GIAR-film. Quantum beat spectra of nuclear resonant scattering obtained after GIAR-film reflection are shifted towards later times with respect to the spectra obtained via direct excitation.

The $^{57}FeBO_3$(3 3 3) reflection has been measured (a) directly and (b) after reflection from the Fe_5B_4C/Ta-based damping-stabilized GIAR-film, showing a temporal shift of $\Delta T = 2.1(1)$ ns compared to the pure $^{57}FeBO_3$(3 3 3) time spectrum. The measurements are displayed in figure 5(b). This shift is explained by the energy dependence of the reflection phase ϕ of the GIAR-film, shown in figure 5(a), together with the energy spectrum of the pure nuclear reflection. For an explanation of the effect it is sufficient to consider only the resonances corresponding to the outer lines of the spectra. The energy difference ΔE between them determines the period $T_B = h/\Delta E$ of the high frequency quantum beats in the time spectra: $T_B = 8.8$ ns for the $^{57}FeBO_3$(3 3 3) reflection. If these resonances are excited via a GIAR-film reflection, their contributions to the scattered field exhibit a phase difference due to the different reflection phases ϕ_1 and ϕ_2 of the GIAR-film at the energies of the resonances. The intensity resulting from the superposition of these contributions is then given by

$$I(t) \propto \sin^2\left[2\pi\frac{t+\Delta T}{T_B}\right] \quad \text{with} \quad \Delta T = \frac{(\phi_1-\phi_2)\,\mathrm{mod}(2\pi)}{2\pi}T_B. \tag{3.3}$$

$T_B = 2\pi\omega_B$ is the quantum beat period. Due to the phase difference $\Delta\phi = (\phi_1 - \phi_2)\,\mathrm{mod}(2\pi)$ a temporal shift of ΔT in the time spectrum appears. In the case of the $^{57}FeBO_3$(3 3 3) reflection, the relative phase between the resonances at $\pm 50\ \Gamma_0$ excited via GIAR-film reflection is $\Delta\phi = 0.45\pi$, see figure 5(a), leading to a shift of $\Delta T = 2.0$ ns. This value is in good agreement with the value derived from the measured data.

Similar quantum beat shifts have been observed in nuclear resonant Laue diffraction [22] and in off-Bragg transmission (forward scattering) [23].

The temporal shift of a quantum beat pattern as reported here is quite analogous to the spatial shift of a interference pattern in two-beam interferometry if the relative phase of the two waves is changed. In principle, this method can be used to map out the complete energy dependence of the phase of a resonant scattering process, especially in case of a strong speedup. This can be realized more conveniently in forward scattering geometry rather than using pure nuclear reflections. Assume two single-line absorbers with resonances slightly separated by a fixed distance in energy. If this compound absorber is energetically tuned relative to the sample under study, the quantum beat shift at each position reveals the phase difference introduced by the sample. As a result, the first derivative of the phase is measured, from which the phase itself can be reconstructed up to an additive constant.

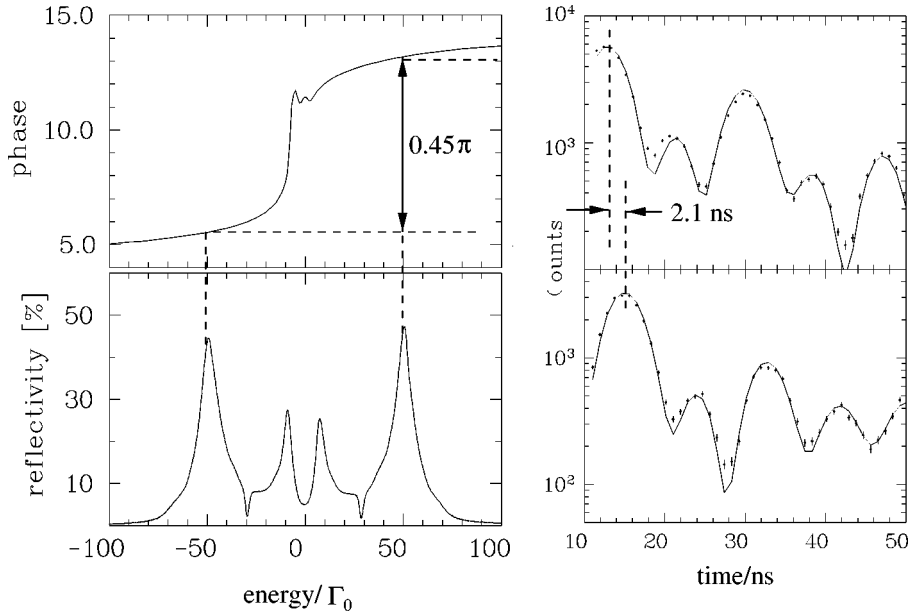

Figure 5. Time spectra of the $^{57}FeBO_3$(3 3 3) reflection excited (a) directly and (b) after reflection from the Fe_5B_4C/Ta-based damping-stabilized GIAR-film. Time spectra of the YIG(0 0 2) reflection excited (c) directly and (d) after reflection from the Fe_2Cr_2Ni/Pd based-damping-stabilized GIAR-film.

3.2. Multilayer superlattices

Very often a hypothetical single crystal composed of alternating layers of ^{56}Fe and ^{57}Fe is taken as a tutorial example to explain the principle of pure nuclear Bragg reflections. With the availability of modern deposition techniques such artificial layered crystals can now be experimentally realized in the form of periodic layer systems with an isotopic magnetic superstructure. Soon after the first experiments with conventional sources, proving the existence of pure nuclear diffraction from such structures [24,25], several of these superlattices have been studied in experiments with synchrotron radiation [26,27], since they exhibit many properties related to the fundamentals of nuclear diffraction and to practical applications in the field of magnetism. The reader is referred to [28] for this subject.

3.3. Reflection gratings

In this section we will show how the transverse coherence of X-rays can be used to produce antireflection devices. These have to be structured in the direction of $\vec{k} + \vec{k}'$ or $\vec{k} \times \vec{k}'$, i.e., perpendicular to $\vec{k} - \vec{k}'$. $\vec{k}$ and $\vec{k}'$ are the wavevectors of the incident and scattered beam, respectively. Laterally structured surfaces have recently been employed in X-ray scattering experiments to characterize the transverse coherence of the radiation field and to study the properties of semiconductor heterostructures [29,30].

For a detailed study, we will here concentrate on reflection gratings with a rectangular profile. The diffraction theory for X-ray reflection gratings has been outlined in [7].

Of particular interest are interference effects in the specular direction, i.e., the zeroth diffraction order. The reflectivity in this order can qualitatively be calculated by coherent superposition of the waves reflected from different parts of a mirror taking into account their relative phases. The structure of a rectangular grating leads to a phase shift between waves reflected from regions on top of or between the grating bars, which depends on the angle of incidence, the thickness of the bars and the refractive index of the material. By proper adjustment of the thickness of the bars, complete destructive interference in the zeroth diffracted order can be achieved. In this way, strong suppression of the nonresonant radiation can be achieved. A strong resonant signal is obtained if the grating surface exhibits, e.g., an isotopic superstructure: due to the phase change of the reflected waves in the resonant scattering process the condition for destructive interference is violated and high reflectivity occurs around the resonance.

However, the above considerations are only meaningful if the transverse coherence length L_T in the plane of the mirror is larger than the lattice constant of the grating. For a mirror illuminated under an angle φ,

$$L_\mathrm{T} = \frac{\lambda D}{\pi h \sin\varphi}, \tag{3.4}$$

where h is the transverse linear dimension of the source and D is the distance of the source from the mirror. The quotient h/D may be viewed as the angular divergence of the radiation. For synchrotron X-rays incident at a few mrad, L_T can easily reach a few hundred μm, so that gratings with macroscopic periods can be used. We now consider a grating with rectangular bars of material 1 of thickness d_1 on a substrate of material 2, see figure 6. The phase shift $\Delta\phi$ between the two waves is then given by

$$\Delta\phi = 4\pi\frac{d_1}{\lambda}\sin\varphi + \big(\phi_{01,1}(\varphi) - \phi_{01,2}(\varphi)\big), \tag{3.5}$$

where $\phi_{01,i}(\varphi)$ is the phase of the Fresnel reflection coefficient $r_{01,i}(\varphi)$ of the medium i. The phase condition that has to be fulfilled for an antireflection grating is simply $\Delta\phi = (2m+1)\pi$. The first term in eq. (3.5) is the geometrical phase shift introduced by the step of height d_1, the second term arises from the different elemental composition of the materials of which the grating is composed. We can neglect the latter term if the surface appears to be homogeneous for nonresonant scattering. This is the case we want to deal with in the following. We further assume the grating bars to contain alternately Fe and ^{57}Fe. For a fixed angle of incidence, this can easily be achieved by proper adjustment of the step height d_1. The condition for equal amplitudes is easily fulfilled if (a) the elemental composition of the grating surface is homogenous or (b) the angle of incidence is below both critical angles of the grating materials. The latter condition leads to only an approximate fulfillment of the amplitude condition

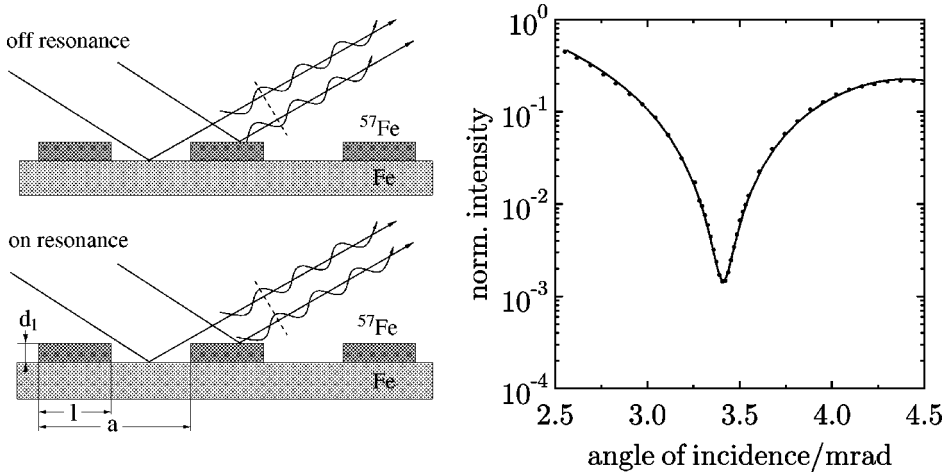

Figure 6. Scheme of a nuclear phase grating: the condition for destructive interference is destroyed around the resonance and resonant reflection occurs. The right part shows the measured angular dependence of the specular reflection (zeroth diffraction order) of a Pd–Pd phase grating with 6.6 nm step height, demonstrating that a strong suppression of electronic scattering can be achieved.

since absorption occurs due to penetration into the medium even below the critical angle.

If case (a) and the phase condition are fulfilled we have a pure antireflection phase grating where the amplitude condition is fulfilled automatically for every angle of incidence if $a = 2l$. This is the case we want to deal with from now on. We further assume the grating bars to contain alternately Fe and ^{57}Fe. Then in the vicinity of a nuclear resonance the antireflection phase condition is violated. The energy dependence of the reflection phase around a single nuclear resonance is shown in figure 1(b). The phase changes significantly between π and 2π, therefore turning destructive interference into constructive interference, which leads to strong resonant reflection.

In order to demonstrate the suppression of the electronic reflectivity, a rectangular Pd/Pd antireflection grating has been produced. The grating thickness was $d_1 = 7.0$ nm with an expected minimum in the 0th order at 3.4 mrad. The grating was produced via sputtering through a mask with a period of $a = 0.2$ mm. This value was chosen because it was smaller than the in-plane transverse coherence length $L_\mathrm{T} = 0.45$ mm of the incident radiation at that angle of incidence. As a substrate, superpolished ZERODUR was used. Especially for grating diffraction a very good surface quality on all length scales is necessary, otherwise the coherence between laterally separated surface elements is lost.

In order to measure the diffraction pattern of the grating, a Si(1 1 1) channel-cut crystal was used as an analyzer. The incident radiation was delivered by a Si(1 1 1) double-crystal monochromator in dispersive setting relative to the analyzer. The experiment was carried out at station F4 at HASYLAB.

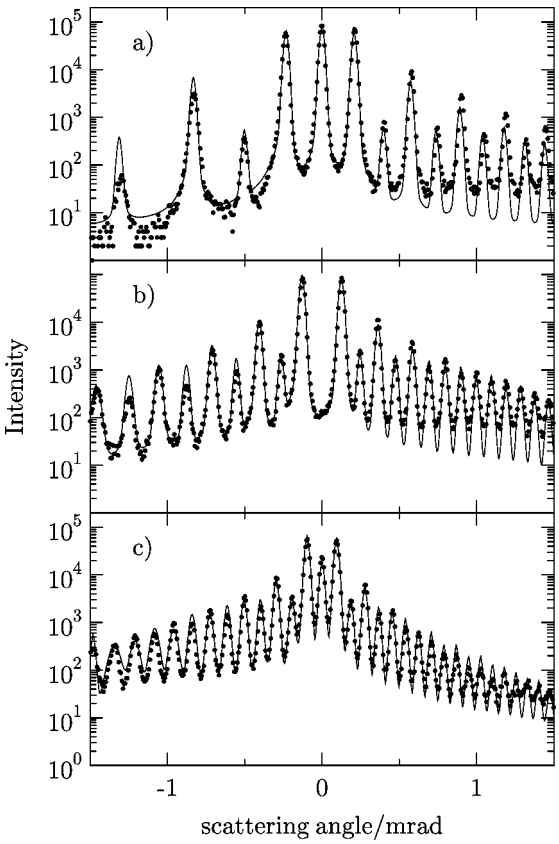

Figure 7. Diffraction at a Pd–Pd phase grating with a thickness of 6.6 nm. The diffraction patterns were taken at angles of (a) 2.0, (b) 3.4, and (c) 4.5 mrad. At 3.4 mrad the specular reflection (zeroth order) is cancelled out by destructive interference. The solid lines are fits according to the dynamical theory outlined in [7,31].

The angular dependence of the diffracted intensity in the specular direction is shown in figure 6. At an incidence angle of 3.4 mrad the intensity dropped by almost three orders of magnitude. At this angle and two neighbouring angles the diffraction pattern was measured, as shown in figure 7. The solid lines are fits according to the dynamical theory outlined in [7], where the slightly trapezoidal shape of the grating bars was taken into account [31].

The experiment shows that the diffraction at this type of gratings can be very satisfactorily explained within the existing theoretical framework. This forms a basis for future applications in nuclear resonant scattering experiments involving these devices. A significant advantage of these antireflection gratings compared with GIAR-films is that for every value of h an angle of incidence can be found for which destructive interference occurs. Moreover, the large angular width of the reflectivity minimum leads to suppression factors that are at least two orders of magnitude larger than those of GIAR-films.

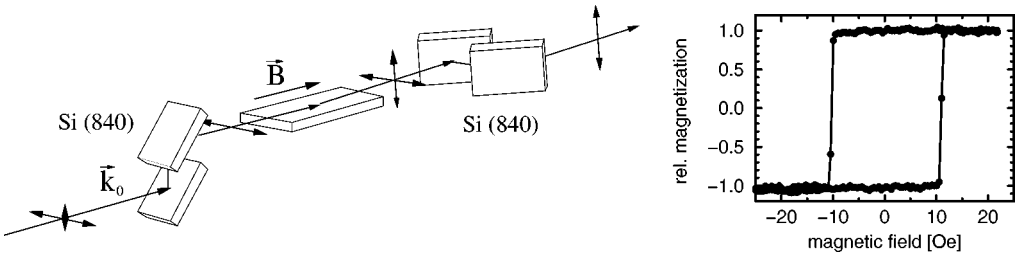

Figure 8. Experimental setup for polarization filtering involving a ^{57}Fe thin-film reflection. The film is magnetized parallel to $\vec{k}_0$ (Faraday geometry). Two Si(8 4 0) channel-cut crystals with a Bragg angle close to 45° provide a polarizer/analyzer pair in crossed setting with a polarization rejection ratio of $\sim 10^{-8}$. The double arrows indicate the relative fraction of σ- and π-polarization in the beam. On the right, a hysteresis loop of a 12 nm thick film of Fe on Si is shown, recorded via the MOKE (Magneto-Optical Kerr Effect) technique.

3.4. Polarization optics

Another possibility for ultra-narrow bandpass filtering is opened by the unique polarization properties of magnetic nuclear resonant scattering. If the degeneracy of the nuclear levels is lifted by a magnetic hyperfine interaction, strong polarization mixing effects are observed, like orthogonal $\sigma \rightarrow \pi$ scattering. Since those effects occur in a narrow range around the resonance energy, a very effective monochromatization can be achieved via polarization filtering of the rotated components. This has been demonstrated in a number of experiments where a polarizer/analyzer setup has been used with an excellent rejection ratio of the unwanted polarization component of up to 10^{-8} [32,33]. For the most efficient use of such a setup, the maximum throughput should be attempted. A close inspection of the magnetic scattering amplitude matrix (see, e.g., [7, eq. (11.7)]) reveals that the strongest orthogonal scattering occurs in Faraday geometry, where the magnetization is aligned collinear with the wavevector of the incident linearly polarized radiation. Such a magnetization can easily be realized with magnetized thin films in grazing incidence geometry. Due to the strong magnetic shape anisotropy, the magnetization of thin films is confined in-plane. Coercive forces are very small so that external fields of a few mT are already sufficient to magnetize ferromagnetic films close to saturation (see figure 8). A typical experimental setup is shown in figure 8. Based on this arrangement, a spectrometer has been developed for μeV-resolved X-ray spectroscopy [34], which is discussed in detail in [35]. In the latter article various layer systems are discussed with respect to their polarization-mixing properties and experimental results are presented.

4. Physics of thin films studied by nuclear resonant scattering

Grazing incidence nuclear resonant scattering has already found a series of applications in thin film physics, mostly dealing with the investigation of multilayer superstructures, see, e.g., [28] and references therein. The sensitivity of the method

can be pushed into the monolayer regime at undulator beamlines of third-generation synchrotron sources [36,37]. The inherent depth sensitivity of grazing incidence reflection enables the study of very thin surface overlayers that result, e.g., from chemical reactions [38]. As a fundamental difference to methods of conventional Mössbauer spectrosopy (e.g., CEMS), this method involves a coherent scattering process and is therefore sensitive to the phase difference between scattering sites. An example of this will be given in the following section. Moreover, the grazing incidence geometry can also be advantageously exploited in the field of inelastic nuclear resonant scattering. This allowed, e.g., a determination of the vibrational density of states of thin films, as will be shown in the last section.

4.1. Magnetism of ultrathin films: Fe-islands on W(1 1 0)

So far in this article, nuclear resonant scattering from thin films has been treated in the isotropic case with no hyperfine interaction present. This was motivated from an instrumentational point of view, not to introduce a complicated energy dependence and time structure to the filtered radiation. On the other hand, the strong dependence on the orientation of internal hyperfine fields leads to interesting applications in thin film and surface magnetism. Here we present an example in the field of thin film magnetism together with some basic considerations.

We start with the reflectivity of a single layer on a semi-infinite substrate as given by eq. (2.3). Since we are discussing films with a very small thickness of only a few monolayers, this equation can be considerably simplified by expanding the exponential, i.e., $\mathrm{e}^{\mathrm{i}2k_{1z}d_1} \approx 1 + 2\mathrm{i}\beta_1 k_{0z} d_1$, resulting in

$$R(\omega) \approx r_{02} + \mathrm{i}\, d_1 t_{02}\big(f_1(\omega) - f_2\big), \tag{4.1}$$

where $t_{02} = 2/(1+\beta_2)$ is the Fresnel transmission coefficient of the vacuum–substrate boundary, and f_i is the nuclear forward scattering amplitude that is related to $\beta_i = \sqrt{1 + 2f_i/k_{0z}}$ [7]. The delayed-time response of the film is then obtained by Fourier transform of eq. (4.1):

$$I(t) = d_1^2 |t_{02}|^2 \big|\tilde{f}_1(t)\big|^2, \tag{4.2}$$

where we have neglected the terms that do not depend on ω since they only contribute to the prompt signal. $\tilde{f}_1(t)$ is the Fourier transform of $f_1(\omega)$. This result allows the following conclusions:

- The maximum contribution occurs at the critical angle of the substrate where $|t_{02}|^2$ peaks, i.e., the thin film is located in an antinode of a standing-wave field that forms above the reflecting surface. See also the discussion in section 2.2.
- The scattered amplitude from the film increases with decreasing photoabsorption in the substrate. This is illustrated in figure 9, where the integral delayed intensity has been calculated for one monolayer of ^{57}Fe on different substrate materials.

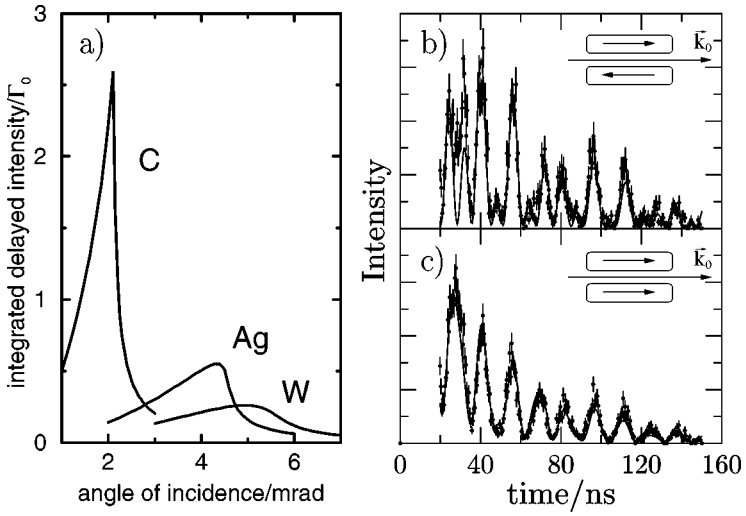

Figure 9. (a) Delayed nuclear resonant scattering from 0.3 nm ^{57}Fe: the intensity peaks at the critical angle of the substrate material. On the right-hand side: time spectra of Fe islands on W(1 1 0): (b) the native state with antiparallel oriented magnetizations, and (c) after remanent magnetization.

To demonstrate the sensitivity of the method, results of experiments with Fe islands on W(1 1 0) are presented here.[4] This system is particularly interesting due to its peculiar growth behavior and the magnetic phenomena associated with it [39–41].

In this experiment, ^{57}Fe films were deposited at 300 K by thermal evaporation of 95%-enriched ^{57}Fe from a crucible under ultra-high vacuum conditions onto a clean single crystal of W(1 1 0). After heating the 5–7 monolayer thick films to about 1000 K, the Fe forms separated and well ordered 3D islands with the lattice constant of bcc bulk iron. The islands are atomically flat on top and of rectangular shape with the long axis pointing along the W[0 0 1] direction. After preparation the tungsten crystal was capped with a carbon film of about 10 nm in order to prevent oxidation of the Fe islands.

The experiments were carried out at the nuclear-resonance beamline ID 18 of the ESRF [42]. The sample was illuminated under an angle of 4.8 mrad, close to the critical angle of W, thereby intercepting a beam cross-section of 0.05 mm $\times$ 2 mm in a vertical scattering geometry. Average delayed count rates of 30 Hz were obtained, allowing us to record time spectra with reasonable statistics within half an hour.

Time spectra of the sample are shown in figure 9. The sample was aligned with the W[0 0 1] axis along $\vec{k}_0$, which implies that the magnetic field of the Fe-islands has the same direction. The sample was first measured in its native state, figure 9(b), and then after remanent magnetization with an external field along W[0 0 1], figure 9(c). The striking difference in both spectra results from different magnetic alignments of

[4] The results presented in this section were obtained in collaboration with J. Bansmann, V. Senz and K.H. Meiwes-Broer, University of Rostock.

the individual islands. The native islands are magnetized antiparallel to each other to minimize the free energy. After external magnetization they are remanently oriented in a parallel alignment. The scattering amplitudes $\hat{f}$ in both cases are considerably different, as can be seen from investigating the scattering amplitude matrix $\hat{f}$ [7, eq. (11.7)]. In the parallel alignment, $\hat{f}$ is nondiagonal and the circular polarizations are the eigenpolarizations of the film, leading to polarization mixing scattering for incident linear polarization. In the native alignment, the superposition of two sublattices with antiparallel orientation results in $\hat{f}$ being diagonal. After Fourier transform into the time domain, we obtain for the time spectra in both cases:

$$I_{\mathrm{mag}}(t) = \left|\widetilde{F}_{+1}(t)\right|^2 + \left|\widetilde{F}_{-1}(t)\right|^2, \tag{4.3}$$

$$I_{\mathrm{nat}}(t) = \left|\widetilde{F}_{+1}(t) + \widetilde{F}_{-1}(t)\right|^2. \tag{4.4}$$

The functions $\widetilde{F}_{+1}(t)$ and $\widetilde{F}_{-1}(t)$ are the time dependent amplitudes emitted from the the transitions with $M = +1$ and $M = -1$, respectively (see [7]).

This experiment demonstrates the strong sensitivity of the method not only to low coverages, but also for phenomena of magnetic ordering. Since the method of nuclear resonant scattering is a local probe of magnetism at the site of the nuclei, yielding the magnitude and the orientational distribution of magnetic fields, it may complement other methods that reveal the macroscopic magnetic moment such as the magneto-optical Kerr effect or X-ray magnetic circular dichroism (XMCD).

4.2. Inelastic nuclear resonant scattering from thin films

In this section it is demonstrated how thin-film interference effects can be employed to significantly increase the intensity of inelastic nuclear resonant scattering [43], so that the vibrational density of states of thin films down to the monolayer level can be obtained. The method relies on constructive interference between multiple reflected waves that leads to the formation of a standing wave between the two boundaries of a thin film. This method becomes particularly effective in the case that the layers under investigation are deposited on substrates of higher electron density. Above the boundary of a total reflecting material, incident and reflected waves superpose to form a standing wave with a period of $D = \lambda/(2\sqrt{\varphi^2 - \varphi_{\mathrm{c}}^2})$, where λ is the wavelength, φ is the angle of incidence, and φ_{c} is the critical angle of the layer material. An intensity enhancement of up to two orders of magnitude, depending on the absorption in the material, can be reached when the layer thickness is an integer multiple of the standing wave period [44].[5] If this condition is fulfilled, energy transport takes place only parallel to the boundaries, i.e., the layer acts as an X-ray waveguide [45,46]. Depending on film thickness, a certain number of guided modes can be excited, which show up as sharp minima in the rocking curve between the critical angles of the layer and the substrate material. The minimum thickness that is required for guided modes

[5] This effect has been used to increase the fluorescence yield in structural studies of layered materials, see, e.g., [44].

to exist is given by $D_{\min} = \lambda/(2\varphi_c)$. The strong suppression of the X-ray reflectivity in these minima has been used in the design of grazing incidence antireflection (GIAR) films, as described in section 3.1. Therefore, the intensity of inelastic scattering, as detected via nuclear fluorescence, can be enhanced by designing the layer system as an X-ray waveguide and coupling the incident beam into a guided mode by proper adjustment of the angle of incidence. The yield of nuclear fluorescence photons generated in a thin film depends on the electric field as a function of depth in the material.[6] This can be determined for an arbitrary layer system through evaluation of eq. (4.14) in [7]. As an example, we calculate the normalized intensity I vs. depth z of a single layer with thickness d, deposited on a total reflecting semi-infinite substrate:

$$I(z) = \left|\frac{E(z)}{E_0}\right|^2 = \left|t_{01}\frac{\mathrm{e}^{\mathrm{i}g_1 z} + r_{12}\mathrm{e}^{2\mathrm{i}gd}\mathrm{e}^{-\mathrm{i}gz}}{1 + r_{01}r_{12}\mathrm{e}^{2\mathrm{i}gd}}\right|^2, \tag{4.5}$$

where $g = n_1 k_0 \varphi$ with n_1 the refractive index of the coating material, k_0 the wavenumber of the radiation and φ the angle of incidence. t_{ij} and r_{ij} are the Fresnel transmission and reflection coefficients of the interfaces between adjacent media, where indices $i, j = 0, 1, 2$ label the vacuum, coating layer, and substrate, respectively. The largest intensity is found in the first order guided modes at $z = d/2$. For Fe on Pd at 14.4 keV, for example, we obtain $I(d/2) \approx 6$. For other Fe containing layer materials with lower critical angle φ_{c1}, values of up to $I(d/2) \approx 40$ are possible. In thin films the absorption of the fluorescence radiation in the sample can be neglected and the fluorescence yield is proportional to the integral over the intensity distribution along the z-coordinate inside the layer [47].

A suitable sample to demonstrate this effect is actually a GIAR-film: at the position of the GIAR-minimum in the rocking curve the incident radiation couples into a guided mode, resulting in an enhanced fluorescence yield. In fact, a GIAR-film consisting of 19 nm $^{57}Fe_2Cr_2Ni$ on Pd has been used in an experiment that was carried out at the Advanced Photon Source (APS), USA. The incident radiation was monochromatized to an energy bandwidth of 5.6 meV. Delayed fluorescence photons were detected by placing the detector (avalanche photodiode, APD) right above the film so that a solid angle as large as possible was subtended. The experimental results are shown in figure 10. A standing wave is excited at 4.1 mrad as indicated by the minimum in the rocking curve displayed in figure 10(a). The intensity distribution as a function of depth at that angle is shown in figure 10(b) with an 5-fold enhancement relative to the incident beam. To demonstrate the enhancement of the inelastic signal, the X-ray energy was tuned 20 meV above the resonance, and the angular dependence of the delayed 6.4 keV fluorescence yield was recorded, shown in figure 10(c). At the location of the maximum a phonon spectrum was recorded within a data acquisition time of just one hour, shown in the inset.

[6] It should be noted that we are dealing here with electronic scattering since the nuclear resonance is excited via phonon energy exchange with radiation that is energetically off resonance.

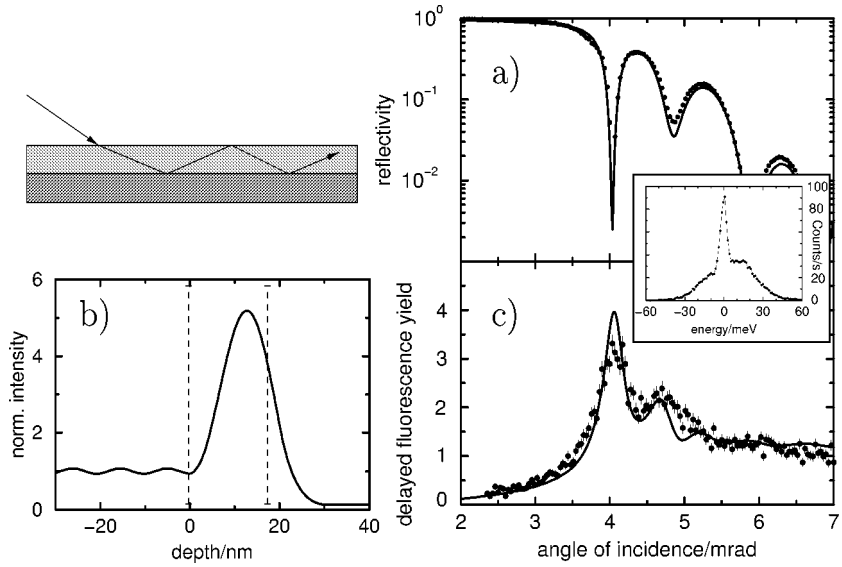

Figure 10. Inelastic nuclear resonant scattering from 19 nm $^{57}Fe_2Cr_2Ni$ on Pd, enhanced by a standing wave inside the film: a first-order guided mode is excited at 4.1 mrad, as indicated by the sharp dip in the measured rocking curve in (a). The corresponding intensity distribution inside the film is shown in (b). In (c) the angular dependence of the delayed nuclear fluorescence yield is shown, normalized to the value at normal incidence. The X-ray energy was tuned 20 meV above the 14.4 keV resonance. The inset shows the phonon spectrum recorded at the peak yield at 4.2 mrad. (Experiment performed at the APS, Argonne Natl. Lab.)

The intensity enhancement due to thin film interference can be even more efficiently used if the investigated film is sandwiched between two total reflecting layers. For example, a 10-fold enhancement of the X-ray intensity was obtained in a $Pd/FeBO_3/Pd$ waveguide structure. As a result, a phonon spectrum from a 13 nm thick layer of vitreous $FeBO_3$ could be recorded, where the ^{57}Fe was contained only in natural abundance (2%), so that the total amount of ^{57}Fe in that sample was equivalent to one monolayer [48]. In other experiments, ^{57}Fe-monolayers have been used to probe the vibrational properties of thin films close to their interfaces [49,50].

5. Conclusion

The development of resonant grazing incidence optics was driven by the search for an effective suppression of nonresonant charge scattering in nuclear scattering experiments. With multilayers and GIAR-films suppression factors in the range of 10^{-2}–10^{-3} have been reached. Limitations are imposed here by surface roughness and layer imperfections. Alternative techniques involve the use of reflection gratings, which have a great potential for even stronger suppression. A completely different approach is the polarization filtering technique, which has shown to reach suppression factors in the range of 10^{-8}. Here, the use of grazing incidence reflection from magnetized thin

films allowed us to obtain maximum values in the throughput. The thin film devices described here may also be very useful in experiments with Mössbauer isotopes other than ^{57}Fe, as has been shown for ^{119}Sn.

Besides the instrumentational aspect, the grazing incidence geometry offers great opportunities for the study of thin-film structures themselves. Particularly exciting are recent experiments at third-generation sources that have demonstrated the monolayer sensitivity of this scattering technique. In addition, the coherence of the scattering process results in a sensitivity to phase differences between scattering sites that is absent in "incoherent" techniques like CEMS.

Finally, interference effects in grazing incidence geometry allow an enhancement of the yield of delayed nuclear fluorescence radiation, which is the signal in the technique of inelastic nuclear resonant scattering. This is an interesting alternative to increasing the flux from the source and may enable us to overcome count rate limitations with existing sources. First experiments that have demonstrated monolayer sensitivity in the determination of vibrational properties of thin films already point in that direction.

Acknowledgements

Most of this work has been performed at the II. Institut für Experimentalphysik (Universität Hamburg) and the Hamburger Synchrotronstrahlungslabor HASYLAB, and parts of it at the ESRF, Grenoble, France, and the APS, Argonne, USA. Many thanks are due to the beamline staff at each place who contributed to the experiments. Especially I want to acknowledge E. Gerdau, O. Leupold, E. Witthoff, E. Lüken, C. Kolbeck, E.E. Alp, T.S. Toellner, R. Rüffer, and E. Burkel for helpful support and many stimulating discussions. Special thanks go to the late M. Harsdorff and his coworkers in the Institut für Angewandte Physik (Universität Hamburg) for their continuous support during preparation of the films. The work described in this article has been funded by the German BMBF under contracts no. 05 5GUAAI 6 and 05 643HRA 5 and in parts by the US Department of Energy, BES Material Sciences, under contract no. W-31-109-ENG-38.

References

[1] S. Bernstein and E.C. Campbell, Phys. Rev. 132 (1963) 1625.
[2] F.E. Wagner, Z. Phys. 210 (1968) 361.
[3] J.C. Frost, B.C.C. Cowie, S.N. Chapman and J.F. Marshall, Appl. Phys. Lett. 47 (1985) 581.
[4] M.A. Andreeva, G.N. Belozerskii, S.M. Irkaev, V.G. Semedov, A.Yu. Sokolov and N.V. Shumilova, Phys. Status Solidi A 127 (1991) 455.
[5] E. Gerdau, R. Rüffer, H. Winkler, W. Tolksdorf, C.P. Klages and J.P. Hannon, Phys. Rev. Lett. 54 (1985) 835.
[6] J.P. Hannon, G.T. Trammell, M. Mueller, E. Gerdau, H. Winkler and R. Rüffer, Phys. Rev. Lett. 43 (1979) 636.
[7] R. Röhlsberger, this issue, section III-1.4.

[8] M. Born and E. Wolf, *Priciples of Optics*, 7th ed. (Pergamon Press, New York, 1978).
[9] A.Q.R. Baron, J. Arthur, S.L. Ruby, A.I. Chumakov, G.V. Smirnov and G.S. Brown, Phys. Rev. B 50 (1994) 10354.
[10] J.P. Hannon, N.V. Hung, G.T. Trammell, E. Gerdau, M. Mueller, R. Rüffer and H. Winkler, Phys. Rev. B 32 (1985) 5068 and 5081.
[11] J.P. Hannon, G.T. Trammell, M. Mueller, E. Gerdau, R. Rüffer and H. Winkler, Phys. Rev. B 32 (1985) 6363 and 6374.
[12] J. Metge, R. Rüffer and E. Gerdau, Nucl. Instrum. Methods A 292 (1990) 187.
[13] S. Kishimoto, Rev. Sci. Inst. 63 (1992) 824.
[14] R. Röhlsberger, Dissertation, Universität Hamburg (1994) and Internal Report, DESY, HASYLAB 94-06 (December 1994).
[15] E. Gerdau, M. Grote and R. Röhlsberger, Hyp. Interact. 58 (1990) 2433.
[16] R. Röhlsberger, E. Gerdau, E. Lüken, H.D. Rüter, J. Metge and O. Leupold, Z. Phys. B 92 (1993) 489.
[17] R. Röhlsberger, O. Leupold, J. Metge, H.D. Rüter, W. Sturhahn and E. Gerdau, Hyp. Interact. 92 (1994) 1107.
[18] R. Rüffer, H.D. Rüter and E. Gerdau, this issue, section IV-1.1.
[19] R. Röhlsberger, E. Gerdau, M. Harsdorff, O. Leupold, E. Lüken, J. Metge, R. Rüffer, W. Sturhahn and E. Witthoff, Europhys. Lett. 18 (1992) 561.
[20] E.E. Alp, T.M. Mooney, T. Toellner, W. Sturhahn, E. Witthoff, R. Röhlsberger, E. Gerdau, H. Homma and M. Kentjana, Phys. Rev. Lett. 70 (1993) 3351.
[21] W. Sturhahn and E. Gerdau, Phys. Rev. B 49 (1994) 9285.
[22] A.I. Chumakov, G.V. Smirnov, M.V. Zelepukhin, U. van Bürck, E. Gerdau, R. Rüffer and H.D. Rüter, Europhys. Lett. 17 (1991) 269.
[23] U. van Bürck, D.P. Siddons, J.B. Hastings, U. Bergmann and R. Hollatz, Phys. Rev. B 46 (1992) 6207.
[24] A.I. Chumakov, G.V. Smirnov, S.S. Andreev, N.N. Salashenko and S.I. Shinkarev, JETP Lett. 55 (1992) 509.
[25] R. Röhlsberger, E. Witthoff, E. Gerdau and E. Lüken, J. Appl. Phys. 74 (1993) 1933.
[26] A.I. Chumakov, G.V. Smirnov, A.Q.R. Baron, J. Arthur, D.E. Brown, S.L. Ruby, G.S. Brown and N.N. Salashchenko, Phys. Rev. Lett. 71 (1993) 2489.
[27] T.S. Toellner, W. Sturhahn, R. Röhlsberger, E.E. Alp, C.H. Sowers and E.E. Fullerton, Phys. Rev. Lett. 74 (1995) 3475.
[28] A.I. Chumakov, D.L. Nagy, L. Niesen and E.E. Alp, this issue, section IV-1.2.
[29] C.A. Lucas and A.P. Firth, Europhys. Lett. 14 (1991) 343.
[30] M. Tolan, G. König, L. Brügemann, W. Press, F. Brinkop and J.P. Kotthaus, Europhys. Lett. 20 (1992) 223.
[31] C. Kolbeck, Diploma thesis, University of Hamburg (1995).
[32] T.S. Toellner, E.E. Alp, W. Sturhahn, T.M. Mooney, X. Zhang, M. Ando, Y. Yoda and S. Kikuta, Appl. Phys. Lett. 67 (1995) 1993.
[33] D.P. Siddons, J.B. Hastings, U. Bergmann, F. Sette and M. Krisch, Nucl. Instrum. Methods B 103 (1995) 371.
[34] R. Röhlsberger, E. Gerdau, R. Rüffer, W. Sturhahn, T.S. Toellner, A.I. Chumakov and E.E. Alp, Nucl. Instrum. Methods A 394 (1997) 251.
[35] R. Röhlsberger, this issue, section VII-2.
[36] L. Niesen, M.F. Rosu, A. Mugarza, R. Coehoorn, R.M. Jungblut, F. Rooseboom, A.Q.R. Baron, A.I. Chumakov and R. Rüffer, Phys. Rev. B 58 (1998) 8590.
[37] J. Bansmann, R. Röhlsberger, V. Senz et al., to be published.
[38] D.L. Nagy, L. Bottyán, L. Deák and E. Szilágyi, Balkan Phys. Lett. 5 (1997) 240.
[39] U. Gradmann, J. Korecki and G. Waller, Appl. Phys. A 39 (1986) 101.

[40] H.J. Elmers, J. Hauschild, H. Fritzsche, G. Liu, U. Gradmann and U. Köhler, Phys. Rev. Lett. 75 (1995) 2031.
[41] H. Bethge, D. Heuer, C. Jensen, K. Reshöft and U. Köhler, Surf. Sci. 331 (1995) 878.
[42] R. Rüffer and A.I. Chumakov, Hyp. Interact. 97/98 (1996) 589.
[43] W. Sturhahn and A.I. Chumakov, this issue, section V-1.1.
[44] Y. Wang, M. Bedzyk and M. Caffrey, Science 258 (1992) 775.
[45] Y.P. Feng, S.K. Sinha, H.W. Deckman, J.B. Hastings and D.P. Siddons, Phys. Rev. Lett. 71 (1993) 537.
[46] S. Lagomarsino, W. Jark, S. DiFonzo, A. Cedola, B. Mueller, P. Engström and C. Riekel, J. Appl. Phys. 79 (1996) 4471.
[47] R. Röhlsberger, W. Sturhahn, T.S. Toellner, K.W. Quast, P. Hession, M. Hu, J. Sutter and E.E. Alp, J. Appl. Phys. 86 (1999) 584.
[48] R. Röhlsberger, W. Sturhahn, T.S. Toellner, K.W. Quast, E.E. Alp, A. Bernhard, J. Metge, R. Rüffer and E. Burkel, Physica B 263–264 (1999) 581.
[49] W. Sturhahn, R. Röhlsberger, E.E. Alp, T. Ruckert, H. Schrör and W. Keune, J. Magn. Magn. Mater. 198–199 (1999) 590.
[50] W. Keune and W. Sturhahn, this issue, section V-1.5.